STRUCTURAL BEHAVIOR OF ASYMMETRIC SPINDLE-SHAPED TENSAIRITY GIRDERS UNDER BENDING LOADS

Rolf H. Luchsinger*, Antje Sydow , René Crettol

Empa, Swiss Federal Laboratories for Materials Science and Technology, Center for Synergetic Structures, Ueberlandstrasse 129, CH-8600 Duebendorf, Switzerland

* Corresponding author. Tel. +41 44 8234090; Fax: +41 44 8234211. e-mail: rolf.luchsinger@empa.ch

Abstract

The load bearing behavior of an asymmetric spindle shaped Tensairity girder is studied experimentally and compared to finite element analyses. The influence of the air pressure on the stiffness of the structure is investigated for homogeneous distributed load, asymmetric distributed load and a local load at the center of the structure. An overall good correlation between experiments and finite element predictions was found. An analytical model based on two coupled ordinary differential equations is presented and solved for the homogeneous distributed load case. The role of the form of the Tensairity girder on the stiffness is investigated by comparing the load-deflection behavior of the asymmetric spindle shaped girder with a cylindrical shaped girder.

Keywords: Tensairity; Lightweight structures; Inflatable structures; Fabrics; Bending load; Full-scale tests;

1. Introduction

Inflatable fabric structures made from plain-woven fabrics combine low weight with compact storage volume, ease to deploy and enhanced damping capabilities. Inflated textile beams (airbeams) can be utilized in a variety of forms to achieve a high level of aesthetics and a free-form design concept and applications ranging from roof structures to inflated airplanes have been demonstrated. In order to understand the load bearing behavior of this unconventional structure, the static response of airbeams under bending loads has been studied [1,2]. Basically, the airbeam behaves as a thin-walled tube structure for small loads. For higher loads compressive stresses exceed the pretension of the hull and wrinkling has to be taken into account [3-6].

Finite elements for predicting the static response of inflated membrane structures were developed [7,8] as well as a Timoshenko beam finite element to predict the deflection and wrinkling load of airbeams at high internal air pressure [9].

A major restriction of airbeams is their poor load bearing capacity which drastically limits their application potential. This deficiency can be overcome by the structural concept Tensairity®, where the airbeam is combined with struts and cables [10]. First applications of Tensairity in the field of civil engineering are roof structures and bridges [11]. In Tensairity, the loads are carried by the struts and the cables while the airbeam stabilizes the system. Thus, minimal cross sections for the compression elements can be used. For example, adding 16 % mass to an airbeam by adding a strut and a cable, the stiffness and ultimate load of the airbeam could be increased through the Tensairity concept by a factor 3 and 4, respectively [12]. Investigations of the static response of spindle shaped Tensairity structures to axial compressive loads revealed their potential as columns without [13] and with internal fabric webs [14]. Tensairity beams were studied under 3-point bending [15] revealing the influence of the air pressure on the stiffness of the structure. It was shown that the forces in the compression and tension member can be reliably estimated by simple analytical formulas. An analytical model for Tensairity beams without web under homogeneous distributed bending load has been proposed recently for thin compression members [16]. Some first results of the load-deflection behavior of web-Tensairity beams indicate that an analytical model based on beam theory can be applied in this case [12].

This study is devoted to the investigation of the static response of asymmetric Tensairity spindles to different types of bending loads. The test specimen and the experimental set up are described in section 2. An analytical model based on the theory of beams on elastic foundation is presented in section 3. Finite element models, outlined in section 4, were developed in a commercial finite element code taking into account the textile's orthotropic linear elastic material properties and geometrical non-linearity. Results and discussion are given in section 5 while section 6 summarizes the main observations of this study and indicates possible further research.

2. Experiments

2.1 Design of the Tensairity beam

The research project started with the objective to demonstrate the major features of Tensairity in a single structure to be featured in a TV show [17]. It was decided to build a mobile demonstration bridge for cars with 8 m span. The challenging specifications demanded, that the two girders of the bridge can be easily transported in the trunk of a small car, that they can be quickly assembled as well as carried by two persons and that the car can finally be driven over the bridge [18]. An asymmetric spindle design was chosen for the girders in order to have a horizontal bridge deck. Aluminum profiles composed of five pieces of equal length of 1.6 m were used for the straight compression element, while steel cables were applied for the tension elements minimizing weight, transport volume and set up time. A test of the Tensairity demonstration bridge is shown in Fig. 1 and a dismantled Tensairity girder of the bridge can be seen in Fig. 2. The weight of a single girder was 68 kg, with 15 kg for the fabric hull, 42 kg for the compression element, 8 kg for the cables and 3 kg for the bolts. Thus, a girder could be carried by two persons. The two girders fitted well in the trunk of the car and were assembled in less than 30 minutes. The load bearing capacity of each girder was initially tested with a concrete block of 860 kg [18].

Fig. 1 Test under operational conditions of the Tensairity demonstration bridge with 8 m span

Fig. 2 Compression element, cables and inflatable hull of a single girder of the Tensairity demonstration bridge with 8 m span

After the show, the load bearing behavior of the girder was tested in detail in our laboratory. To this end, the segmented aluminum compression elements were replaced by a single steel compression element while the original hull and cables of the test bridge were used. Geometry and dimensions of the girder are shown in Fig. 3. The straight compression member is a rectangular, hollow steel section of 120 mm x 40 mm x 3 mm. It is placed in a fabric pocket fixed along the top of the membrane within which it is held by friction due to air pressure in the hull. The fabric hull defines the shape of the girder. It has an inclined circular cross section of diameters changing between 150 mm at the ends and 600 mm at the centre line. The membrane is made of PVC-coated polyester fabric (Valmex 7318 by Mehler Texnologies) with a thickness of 0.85 mm and a weight of 1000 g/m^2. The fabric orientation was chosen such that the warp direction corresponds to the longitudinal direction of the membrane body. Six spiraling cables were used as tension members, all of them connected at both ends to the compression element. The two long cables span 7.8 m and cross each other at the centre line underneath the membrane body. The four short cables, two on each half of the girder, span 3.5 m. Made of 6 x 7 stainless steel wire ropes, the long cables have a diameter of 8 mm and an effective area of 29.1 mm^2, while the shorter ones have a diameter of 6 mm and an effective area of 15.7 mm^2. The Young's modulus of the cables is 100 kN/mm^2. The elastic properties of the fabric were measured in house with our biaxial test rig [19] and found to be E_{warp} = 1.06 kN/mm^2, E_{fill} = 0.53 kN/mm^2, G = 0.018 kN/mm^2 and ν = 0.386.

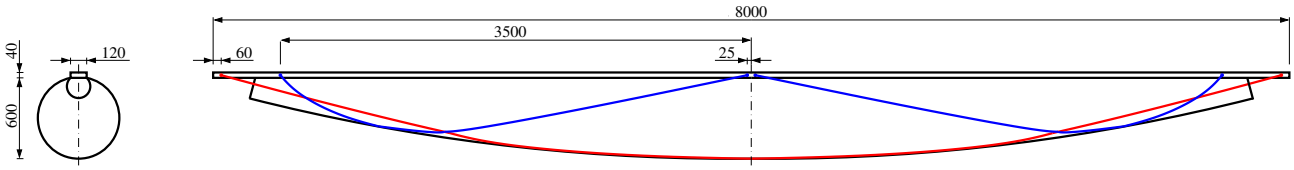

Fig. 3 Dimensions of the asymmetric Tensairity spindle

2.2 Test rig

A dedicated test rig was set up at Empa for the experimental investigations of the load bearing behavior of the Tensairity girder (Fig. 4). Different load cases were considered: local load at the centre of the girder, homogeneous distributed load and asymmetric distributed load. The local load was applied by a force controlled winch, while two hydraulic pistons instrumented with load cells and a whippletree system with two balance layers and a system of four rollers transferring the force to the compression member was used to

generate distributed loads as shown in Fig. 5 [20]. Only one actuator was used to generate the asymmetric distributed load. The vertical deformation was recorded by seven displacement transducers spaced equally along the length of the beam. The cable load was measured with load cells connected to selected cables. The internal air pressure was controlled by a manometer and recorded by a pressure gauge. Experiments were conducted at 10 kPa, 20 kPa, 30 kPa and 40 kPa. The air pressure was kept constant during the measurement. The signals of all measurement devices were collected by a data acquisition system and processed to provide the loading information and resulting forces together with the measured displacements.

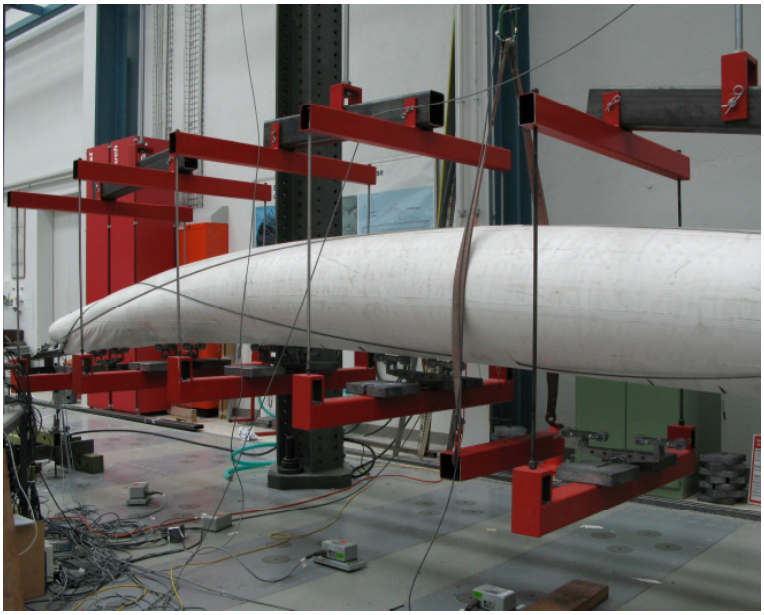

Fig. 4 Test rig for the asymmetric Tensairity spindle

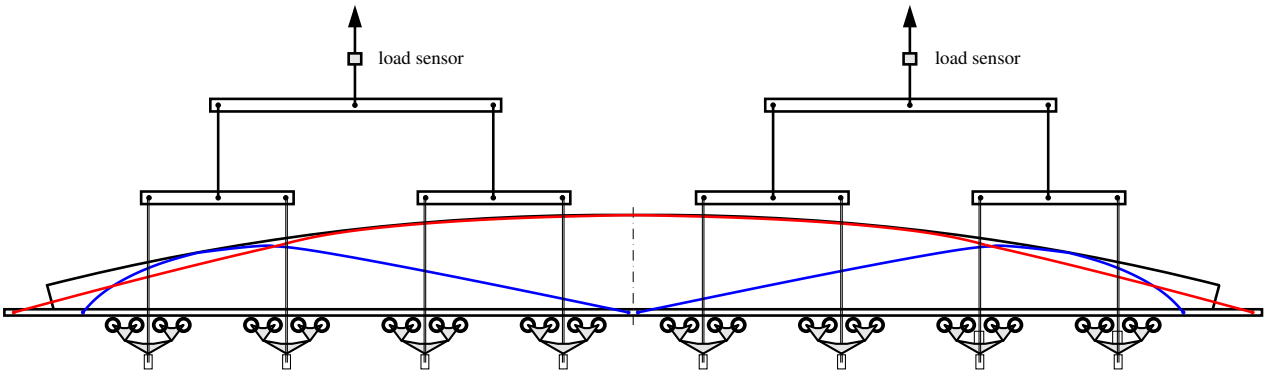

Fig. 5 Whippletree system to generate distributed loads

Given the experimental set up with the whippletree system, the load was applied by pulling the structure against the direction of gravity and the Tensairity beam was placed into the test rig upside down. The beam was supported in the centre during inflation, then the cables were tensioned and the support removed before

the loading started. Typically the load was applied in four steps until maximum load and was kept constant for 5 minutes for each load step to allow the structure to settle.

3. Analytical Model

In order to develop an analytical model for the Tensairity spindle, the system needs to be simplified in various ways. The basic idea of the model is to consider the inflated hull as an elastic foundation with an air pressure dependent modulus [14] which couples the compression with tension elements [16, 20]. Since only homogeneous distributed loads are considered in the model, it can be assumed that the horizontal force component along the cable and the compression element is constant and of equal magnitude. The short cables can be neglected for the homogeneous distributed load. It is assumed, that the long cables lie in the symmetry plane with the compression element and have a parabolic shape given by the contour of the hull. This way the three dimensional structure of the girder is reduced to a two dimensional problem.

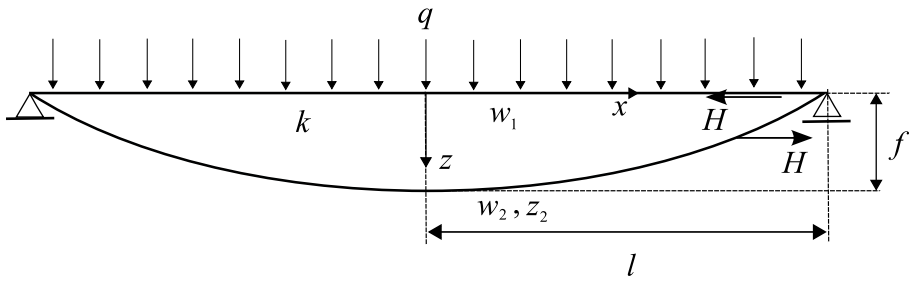

Fig. 6 Sketch of the components of the analytical model.

The configuration and the coordinate system are defined in Fig. 6. Based on beam theory, the ordinary differential equations for the compression and the tension element are given by

$$EI \cdot \frac{d^4 w_1}{dx^4} + H \cdot \frac{d^2 w_1}{dx^2} + k \cdot (w_1 - w_2) = q \tag{1}$$

$$-H \cdot \frac{d^2 (w_2 + z_2)}{dx^2} - k \cdot (w_1 - w_2) = 0 \tag{2}$$

where EI is the bending stiffness of the compression element, q the homogenous distributed load, H the horizontal force component and w_1 and w_2 the vertical displacement of the compression element and tension element, respectively. The modulus of the elastic foundation is given by $k = \pi \cdot p/2$, where the factor 2 stems from the fact that the cable is the reference point and not the center line of the spindle as it was the case

in the analytical model for the axial compression of Tensairity girders [13]. The cable z_2 is approximated to have a parabolic shape given by

$$z_2 = f \cdot \left(1 - \left(\frac{x}{l}\right)^2\right) \tag{3}$$

where f is the diameter of the spindle at midspan and l half of the span of the girder.

Solving Eq. (1) for w_2 yields

$$w_2 = w_1 - \frac{q}{k} + \frac{H}{k} \cdot \frac{d^2 w_1}{dx^2} + \frac{EI}{k} \cdot \frac{d^4 w_1}{dx^4} \tag{4}$$

and substitution into Eq. (2) results in the 6th order differential equation

$$\frac{d^6 w_1}{dx^6} - \lambda^2 \cdot \frac{d^4 w_1}{dx^4} = -\frac{k}{EI} \cdot \left(\frac{q}{H} - \frac{2 \cdot f}{l^2}\right) \tag{5}$$

where the abbreviation

$$\lambda = \sqrt{\frac{k}{H} - \frac{H}{EI}} \tag{6}$$

has been introduced. Solving Eq. (5) leads to

$$w_1 = \frac{1}{\lambda^4} \cdot C_0 \cdot \cosh(\lambda \cdot x) + C_1 \cdot x^4 + C_2 \cdot x^2 + C_3 \tag{7}$$

and with Eq. (4) to

$$\begin{aligned} w_2 = &-\frac{q}{k} + C_0 \cdot \left(\frac{1}{\lambda^4} + \frac{H}{k \cdot \lambda^2} + \frac{EI}{k}\right) \cdot \cosh(\lambda \cdot x) + C_1 \cdot x^4 + \left(C_2 + \frac{H}{k} \cdot 12 \cdot C_1\right) \cdot x^2 + \ldots \\ &C_3 + \frac{2 \cdot H}{k} \cdot C_2 + \frac{EI}{k} \cdot 24 \cdot C_1 \end{aligned} \tag{8}$$

where symmetry $w_1(x) = w_1(-x)$ was implied.

The four coefficients C_0, C_1, C_2 and C_3 are determined by the three boundary conditions $w_1(l) = 0$, $w_2(l) = 0$, $d^2 w_1 / dx^2\big|_{x=l} = 0$ together with Eq. (5). One obtains

$$C_0 = \frac{k}{EI \cdot \lambda^2 \cdot \cosh(\lambda \cdot l)} \cdot \left(\frac{-q \cdot H}{EI \cdot k} + \frac{2 \cdot f}{l^2}\right) \tag{9}$$

$$C_1 = \frac{k}{24 \cdot EI \cdot \lambda^2} \cdot \left(\frac{q}{H} - \frac{2 \cdot f}{l^2}\right) \tag{10}$$

$$C_2 = -\frac{C_0}{2 \cdot \lambda^2} \cdot \cosh(\lambda \cdot l) - 6 \cdot C_1 \cdot l^2 \tag{11}$$

$$C_3 = -\frac{C_0}{\lambda^4} \cdot \cosh(\lambda \cdot l) - C_1 \cdot l^4 - C_2 \cdot l^2 \tag{12}$$

The last parameter to be determined is *H*. Assuming that the increase of the cable length due to the deformation matches the elastic elongation due to the cable force, one obtains [16]

$$\frac{H \cdot s_0}{E_2 A_2} = \frac{2 \cdot f}{l^2} \cdot \int_0^l w_2 \cdot dx \tag{13}$$

where the length reduction of the compression element has been neglected due to the much higher cross sectional area compared to the cables. The parameter $s_0 = l + (2 \cdot f^2)/(3 \cdot l) \approx l$ is the initial cable length and E_2A_2 is the stiffness of the cables. The integral is calculated to

$$\begin{aligned} \int_0^l w_2 \cdot dx = & \left(-\frac{q}{k} + C_3 + \frac{2 \cdot H \cdot C_2}{k} + \frac{24 \cdot EI \cdot C_1}{k} \right) \cdot l + \ldots \\ & \frac{C_0 \cdot \sinh(\lambda \cdot l)}{\lambda} \cdot \left(\frac{1}{\lambda^4} + \frac{H}{k \cdot \lambda^2} + \frac{EI}{k} \right) + \frac{C_1 \cdot l^5}{5} + \left(C_2 + \frac{12 \cdot H \cdot C_1}{k} \right) \cdot \frac{l^3}{3} \end{aligned} \tag{14}$$

The horizontal force is obtained by numerically solving Eq. (13). Given *H,* the four coefficients and thus the displacements w_1 and w_2 are given.

Further simplifications can be made for the Tensairity girder at hand. It can be shown, that

$$w_1(0) \approx w_2(0) + \frac{q}{k} \tag{15}$$

that is, the last two terms of the right hand side of Eq. (4) are very small for the given system and can thus be neglected. Furthermore, by approximating the displacement of the cable by a parabola

$$w_2(x) \approx w_2(0) \cdot \left(1 - \left(\frac{x}{l} \right)^2 \right) \tag{16}$$

and with the horizontal force approximated by [10]

$$H_0 = \frac{q \cdot l^2}{2 \cdot f} \tag{17}$$

one obtains with Eq. (13)

$$w_1(0) = \frac{q}{k} + \frac{3}{16} \cdot \gamma \cdot \varepsilon_2 \cdot L \tag{18}$$

$$w_2(0) = \frac{3}{16} \cdot \gamma \cdot \varepsilon_2 \cdot L \tag{19}$$

where the slenderness $\gamma = L/f$, the span $L = 2 \cdot l$ and the strain of the cable $\varepsilon_2 = H_0 / E_2 A_2$ have been introduced. The stiffness defined as $m_1 = q \cdot L / w_1(0)$ is

$$m_1 = \frac{1}{L \cdot \left(\frac{1}{k \cdot L^2} + \frac{3 \cdot \gamma^2}{128 \cdot E_2 A_2} \right)} \tag{20}$$

For small air pressure values, the stiffness is dominated by the squeezing of the inflated tube while for high pressure values the elasticity of the cable dominates the stiffness. The air pressure at which both effects contribute equally is given by

$$p_c = \frac{256}{3} \cdot \frac{E_2 A_2}{\pi \cdot \gamma^2 \cdot L^2} \tag{21}$$

The displacement w_1 and w_2 under a homogeneous distributed total load of 6 kN and an air pressure of 20 kPa is shown in Fig. 7. The linear solution (Eqs. (16), (18) and (19)) underestimates the displacement of the full solution (Eqs. (7) and (8)) which can also be seen in the load-displacement behavior at midspan for an air pressure of 20 kPa (Fig. 8), where the non-linear behavior of the full solution can be seen. The linear solution might only be seen as a rough estimate in the present case.

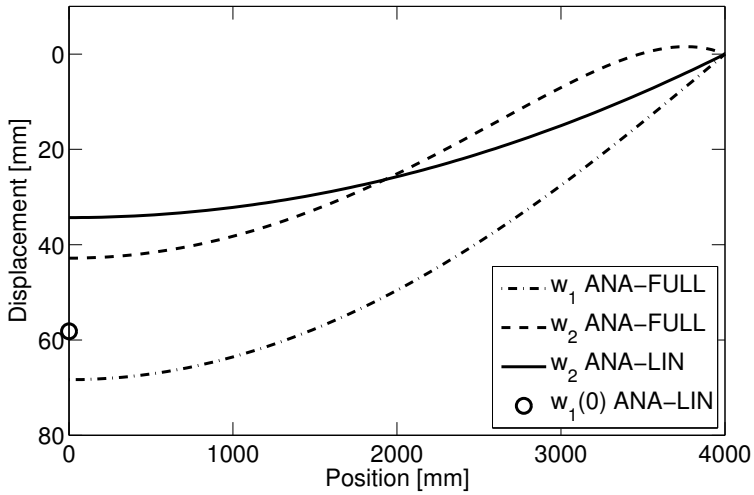

Fig. 7 Analytical displacement of the full and the linear solution for a total load of 6 kN and an air pressure of 20 kPa.

The displacements w_1 and w_2 diverge for $\lambda = 0$. Thus, the critical horizontal force is determined by Eq. (6)

$$H_c = \sqrt{k \cdot E \cdot I} \tag{22}$$

Together with Eq. (17), the total critical load $Q_c = q_c \cdot L$ can be written as

$$Q_c = \frac{8}{\gamma} \cdot \sqrt{\frac{\pi \cdot p \cdot E \cdot I}{2}} \tag{23}$$

which will give an estimate of the maximal applicable load.

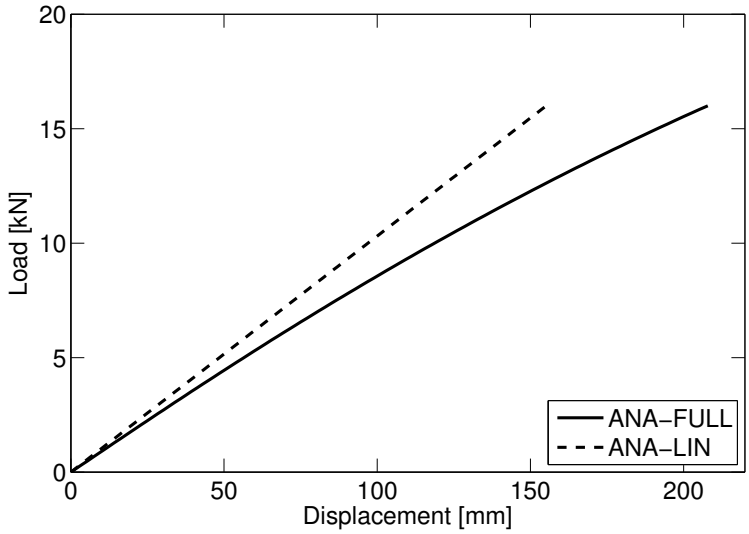

Fig. 8 Load-displacement behavior of the full and the linear solution for a pressure 20 kPa.

4. Finite Element Model

The finite element modeling was carried out in ABAQUS/Explicit version 6.9. For the compression member 4-noded shell elements with reduced integration (S4R) were used, while 4-noded membrane elements with reduced integration (M3D4R) and 3-noded membrane elements (M3D3) were used for the membrane. The cables are modeled with 2-noded linear truss elements (T3D2). The structure is constrained with simple supports on the beam ends undersides. The membrane is tied to the beam. Other movements are restricted by contact formulations. The FEM model of the Tensairity girder is shown in Fig. 9.

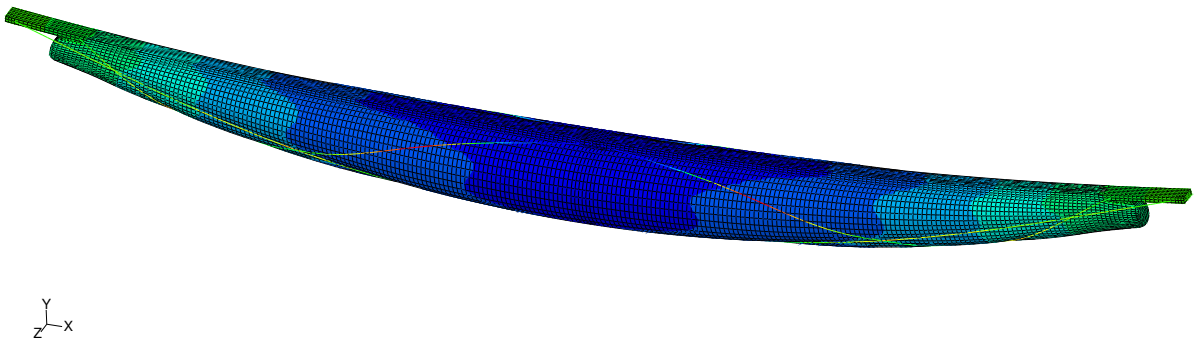

Fig. 9 FEM model of the Tensairity girder with an applied homogeneous load

Contact was calculated by a penalty algorithm preventing vertical penetration of the parts but allowing for separation and sliding with friction in tangential directions. The first contact zone was defined between the compression member and the membrane pocket, where the friction parameter was set to 0.05 during inflation and to 0.1 after inflation. The second contact zone was defined between the cables and the membrane. Inflation was considered to be frictionless, while the friction parameter was set to 0.5 during loading. A low numerical damping was used to suppress vibrations of the structure.

Homogeneous and asymmetric distributed loads were applied to the compression element by 32 and 16 equal point loads as given by the experimental set up of Fig. 5, respectively, where each of the rollers is modeled as one point load. The actual position of the cables in contact with the hull was determined by FEM. A starting configuration of the cables was defined by a series of straight lines not in touch with the hull that follows approximately the expected path. An artificial temperature load was then applied to the cables that shrinks them to their actual length and forces them into the correct position in contact with the membrane. The loading of the structure in the FEM analysis was done in three steps: (1) inflation of the hull and temperature loading of the cables to determine the initial configuration, (2) gravity loading and (3) external loading.

5. Results and Discussion

5.1 Validation of the FE-Model

To investigate the convergence behavior of the FEM analysis, calculations with different levels of discretization were performed. The stiffness of the beam for different air pressure values is shown in Fig. 10. It can be seen that the results are well converged for 18820 nodes which will be used in subsequent calculations. Further convergence tests have shown that the numerical results converge well when the loads for each step are applied smoothly within one second.

The cable prestress is applied in the FEA by the cooling temperature as described above. This cooling temperature is not a physical parameter and its influence needs to be investigated. The load-displacement behavior for different cable lengths due to different cooling temperatures is shown in Fig. 11 for homogenous loading and an air pressure of 20 kPa. The standard FEA configuration with a cable length of 8070.5 mm / 3718.2 mm (long/short) is compared to a configuration with a slightly reduced cable length

by -11.1 mm / -7.7 mm (long/short) in prestress 1 and with a slightly increased cable length by + 10.8 mm / +7.7 mm (long/short) in prestress 2. Different cable lengths lead essentially to a parallel shift of the curve in the displacement direction while the slope can be considered as independent. The same behavior was found for other air pressure values.

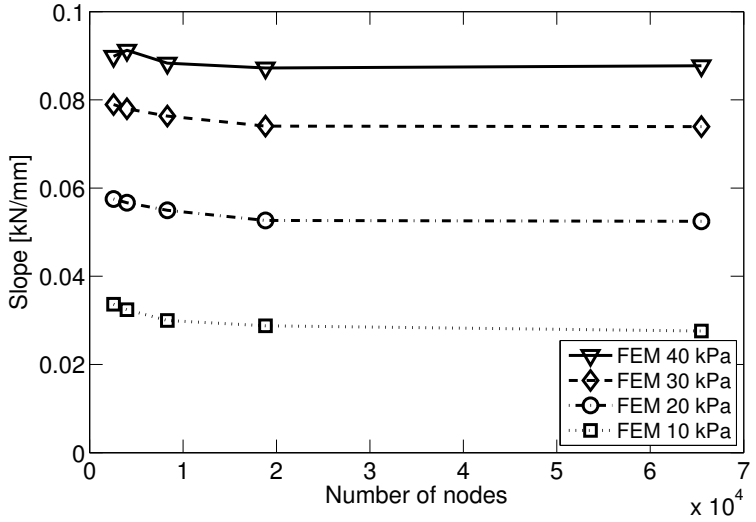

Fig. 10 Convergence test of the FEM analysis for homogeneous loading

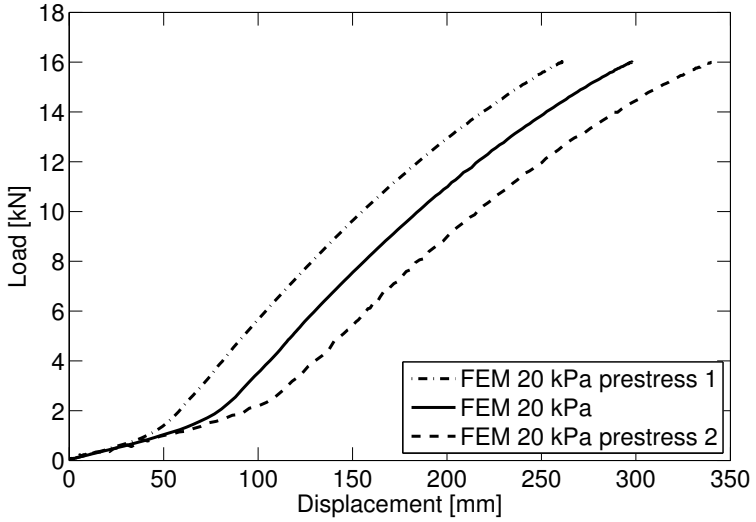

Fig. 11 FEA load-displacement behavior for different initial cable lengths

5.2 Homogeneous distributed load

The design of the asymmetric spindle shaped Tensairity girder is well adapted to homogeneous distributed loads. The displacement along the length of the compression element for an air pressure of 20 kPa and a total applied load of 11 kN is shown in Fig. 12. The FEM results show slightly smaller deflections at the center part of the girder compared to the experimental data but overall, FEA and experiment correspond

well. The corresponding load-displacement curves at midspan of the compression element are given in Fig. 13 for the two air pressure values 20 kPa and 40 kPa. The stiffness increases for the initial loads due to the experimental arrangement, where the applied load acts against gravity. The first load steps are used to compensate the weight of the girder, before a rather linear behavior denotes the stiffness of the Tensairity structure. The FEM predictions for the loading match well with the experimental results for both pressure values. For the experimental results, both loading and unloading are shown. A hysteretic behavior was found which has been reported earlier for local loads [15] and seems to be typical for Tensairity girders.

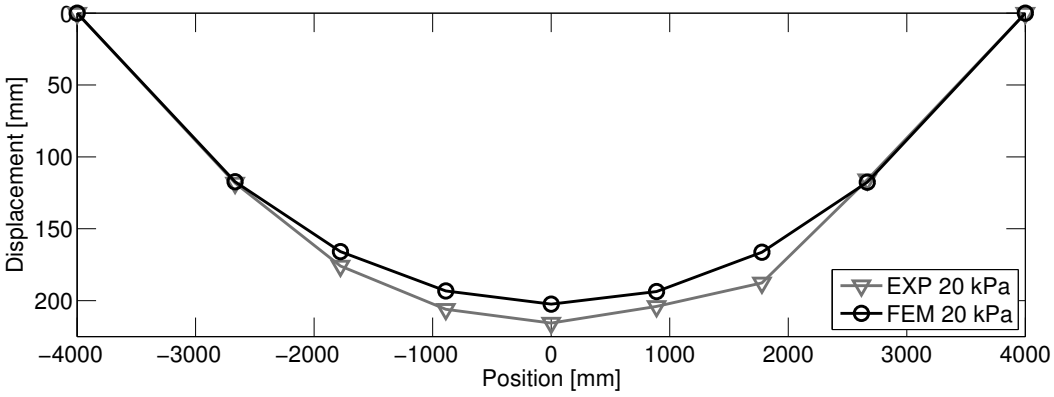

Fig. 12 Displacement along the length of the compression member at 20 kPa for homogeneous distributed load of 11 kN

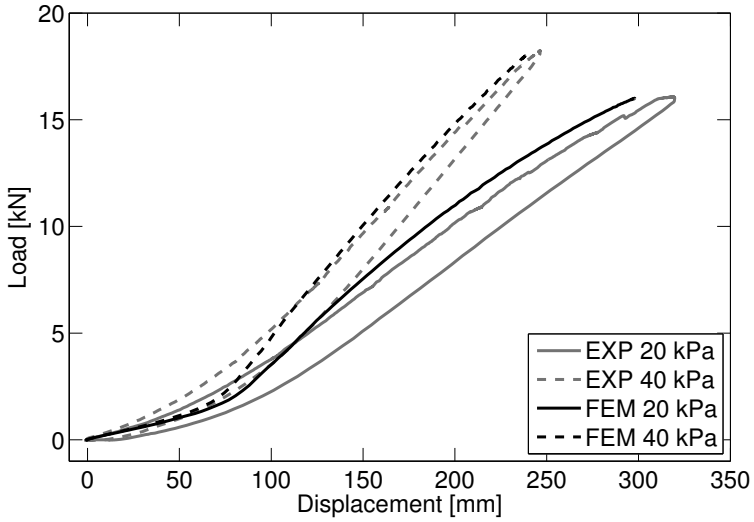

Fig. 13 Load-displacement behavior at the center of the compression member for 20 kPa and 40 kPa for homogeneous distributed loading

The slope of the load-displacement behavior is shown in Fig. 14. The slope was defined for the experimental, FEM and analytical results by a linear fit to the load-displacement curve between 6 kN and 1 kN below the maximal applied experimental load value. As expected from Fig. 13, the experimental and numerical slopes correspond well for all four pressure values investigated. The full solution of the analytical

model based on Eqs. (7)-(14) overestimates the experimental results by about 10% to 20%. One possible reason for the higher stiffness of the analytical solution is the simplified treatment of the cables and the hull in the model. The analytical solution of the linear model for the slope (Eq. (20)) is also plotted in Fig. 14. As expected from Fig. 8, the linear solution predicts a higher stiffness than the full solution. It is about 40% higher than the experimental result for an air pressure of 40 kPa. Nevertheless, the dependency of the slope on the air pressure is well mirrored with the linear model. The simple model might serve as a first, but optimistic estimate of the stiffness of the asymmetric Tensairity girder.

The air pressure p_c (Eq. (21)) is determined to be 14 kPa for the given girder. The linear theory confirms the general experience that air pressure values in the order of 10 - 20 kPa are typically enough for Tensairity girders to cope with distributed loads. The critical load defined in Eq. (23) is 25 kN for a pressure of 20 kPa which is about 9 kN higher than the maximal applied load in the experiment at this pressure value.

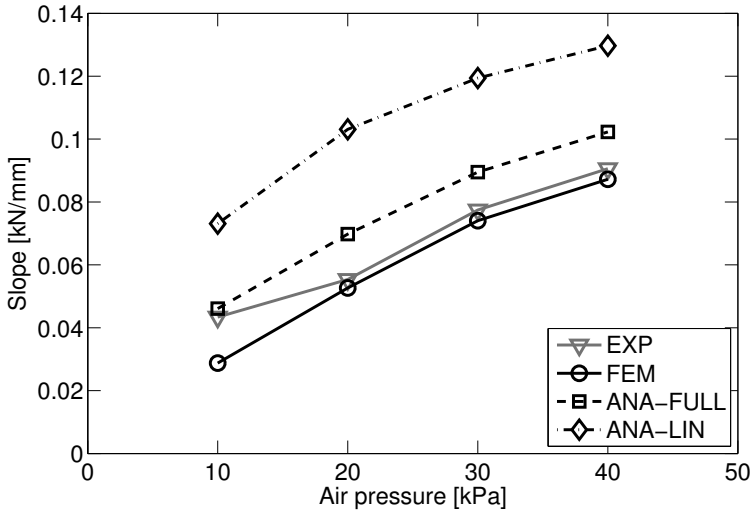

Fig. 14 Slope of the load-displacement curve as a function of air pressure for homogeneous distributed load

5.3 Central local load

The displacement of the compression element along the span for a local load of 6 kN at midspan and an air pressure of 20 kPa is shown in Fig. 15. Both experimental and FEM results are given. The load-displacement behavior at midspan (Fig. 16) reveals a good match between the numerical and experimental data especially for loads above 4 kN. The experimental and FEM slopes (Fig. 17) correspond well for all four air pressure values investigated. At 20 kPa, the experimental slope is 0.040 kN/mm. In the case of a homogeneous distributed load, the corresponding slope is 0.055 kN/mm and the ratio between the slope of the local load

and the homogenous load is 0.727. At 40 kPa, this ratio is 0.598. For girders with constant cross section, beam theory predicts a ratio of 0.625 which is in the same range.

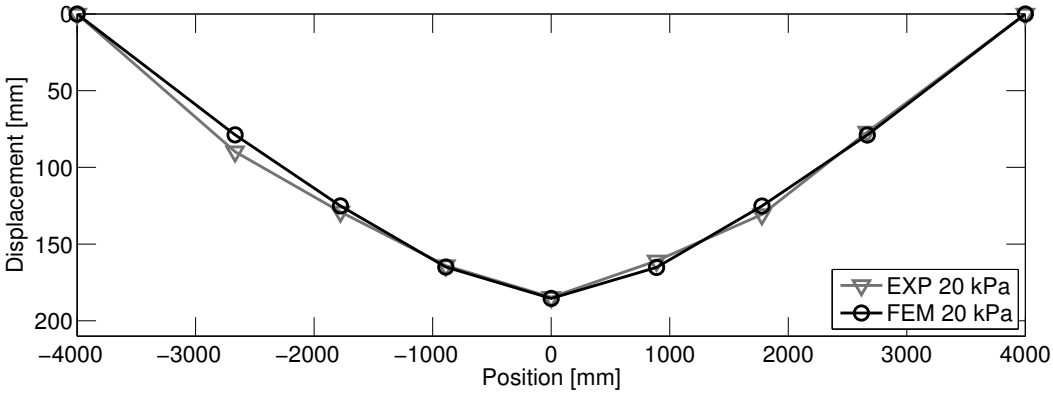

Fig. 15 Displacement along the length of the compression member at 20 kPa for central local load of 6 kN

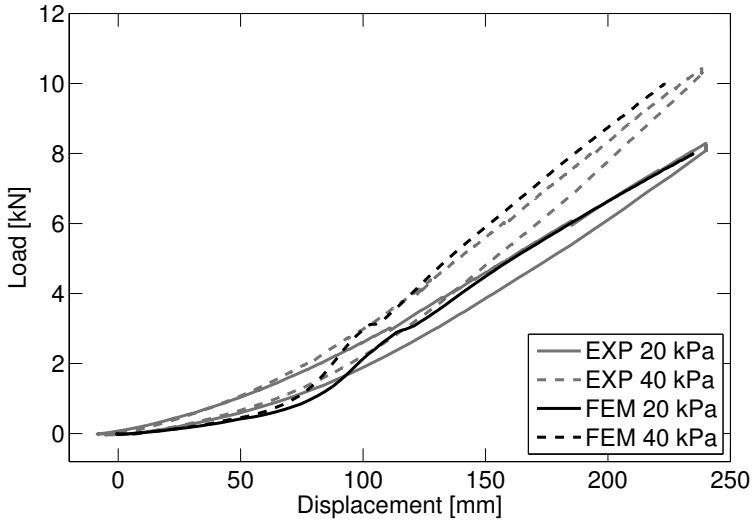

Fig. 16 Load-displacement behavior at the center of the compression member for 20 kPa and 40 kPa for central local load

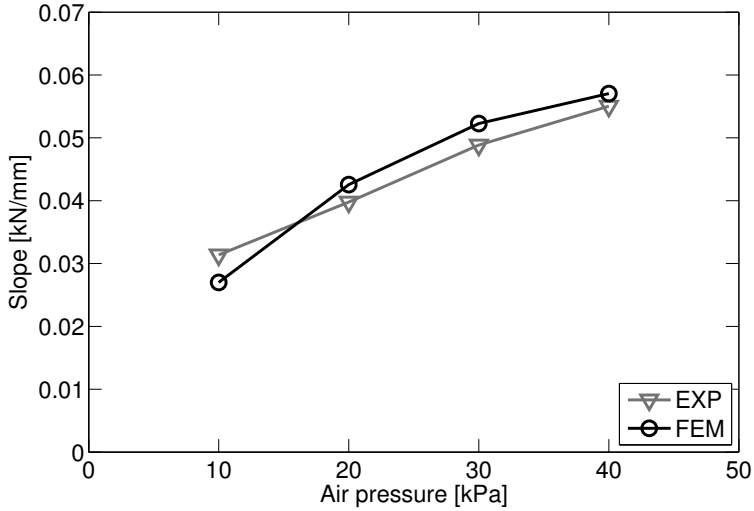

Fig. 17 Slope of the load-displacement curve as a function of air pressure for central local load.

5.4 Asymmetric distributed load

The displacement along the span for an asymmetric distributed load of total 6 kN on the left half of the girder is shown in Fig. 18. The air pressure is set to 20 kPa. FEM results and experimental results compare reasonably well. The maximum displacement of 104.5 mm for a load of 6 kN is found at about a distance of 1.32 m from the center. The corresponding homogeneous distributed load of 1.5 kN/m leads to a displacement of 230 mm at midspan.

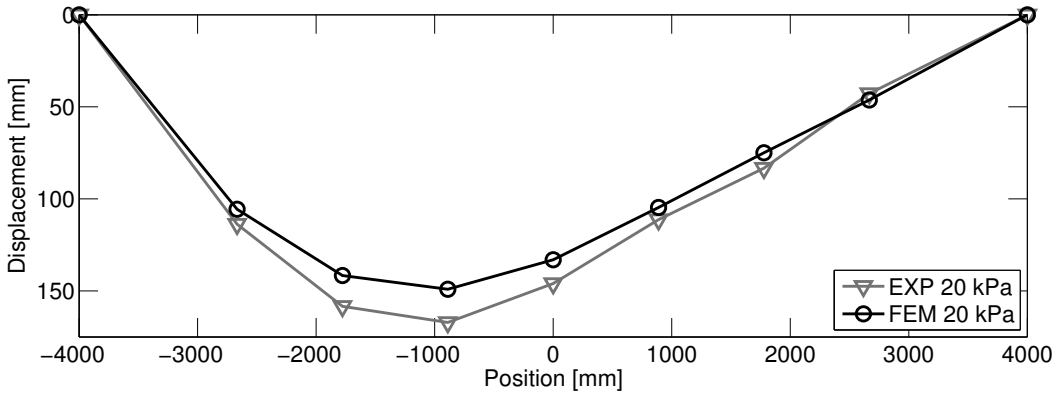

Fig. 18 Displacement along the length of the compression member at 20 kP for asymmetric distributed load of 6 kN

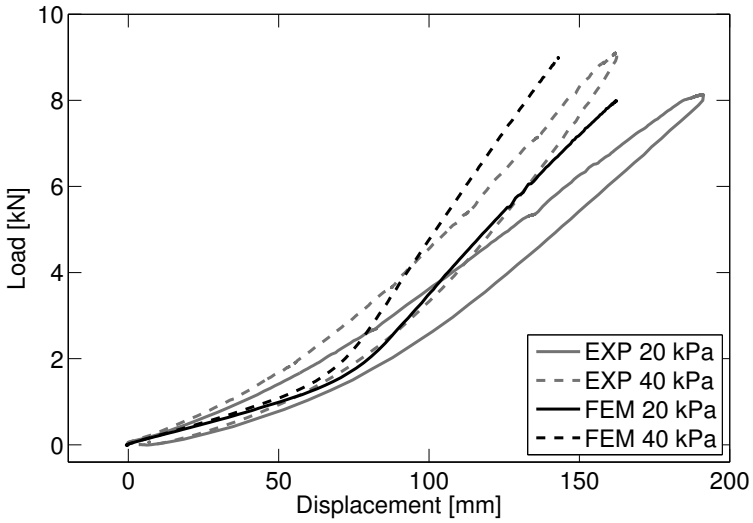

Fig. 19 Load-displacement behavior at the center of the compression member for 20 kPa and 40 kPa for asymmetric distributed load

The load-displacement response at midspan as given in Fig. 19 reveals that FEM predicts a stiffer structure in this load case. This is also reflected in Fig. 20, where the corresponding slopes are presented. The FEM values are up to 37 % higher than the experimental values. A possible reason for this discrepancy is gliding of the compression element in the hull pocket as well as gliding of the cables on the hull surface in the experiment. Such behavior was observed for small Tensairity girders under asymmetric loading. These

effects depend on the friction coefficients and are not easy to model precisely. Nevertheless, the overall correspondence between FEM and experimental data can still be considered as reasonably good.

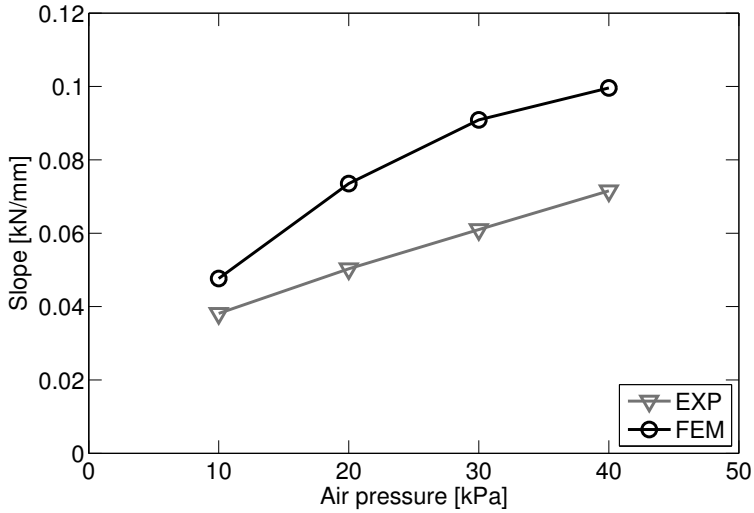

Fig. 20 Slope of the load-displacement curve as a function of air pressure for asymmetric distributed load

5.5 Cable tension

The cable load can be estimated by assuming that the maximal bending moment is compensated by the moment due to the cable tensioning and the distance to the compression element. The ratio of the load of the two long cables to the total applied load is determined by the slenderness and given as $\gamma/8$ for the homogeneous distributed load and $\gamma/4$ for the symmetric local load [15] with γ = 13.3. For asymmetric distributed load, the maximal moment is given at $3/8 \cdot L$ and one obtains for the ratio of the cable force to the applied load $\gamma/7$. A linear relation was found between the cable force and the applied load mainly independent of the air pressure in all load cases confirming the results of a previous study with a symmetric spindle shaped Tensairity girder under local load [15].

The ratio of the cable load to the applied load is summarized in Tab. 1 for the long and the short cables. The experimental values for the short cables on the side where the asymmetric load is applied are given. The tension of the short cables is small for the local load and for the homogeneous distributed load. In the case of the asymmetric distributed load, the tension in the short cables underneath the load reaches about 14% of the force in the long cables while the value of the unloaded side is 0.006 and thus negligible. Indeed, the short cables were introduced in order to accommodate the asymmetric loads when the front wheels of the car are moving on the deck of the demonstration bridge. A reasonable match is found between experiment and the analytical estimate for the long cables in all three load cases.

	long cable			short cable	
	Experiment	FEM	Theory	Experiment	FEM
Hom. distr. load	2.00	1.63	1.66	0.09	0.23
Sym. loc. load	2.57	2.22	3.33	0.06	0.12
Asym. distr. load	1.84	1.44	1.90	0.25	0.30

Table 1 Ratio of cable force over total load for the long and short cables.

5.6 Spindle versus cylinder

The first built Tensairity girders had a cylindrical shape. The cylindrical shape has some advantages as the hull is easy to design and fabricate. On the other hand, the spindle shape leads to a more attractive design, significantly less fabric material is used and a simpler design when positive and negative loads need to be carried [15]. Furthermore, based on numerical studies it was concluded that the spindle shape leads to a stiffer structure [21]. In order to verify this aspect experimentally, a cylindrical shaped Tensairity girder with a constant diameter of 0.6 m was built and tested. The same compression element as for the asymmetric spindle girder was used and the cable configuration was identical while the length of the all cables had to be adjusted. Experiments as well as FEM calculations were conducted for all three load cases and air pressure values of 10 kPa, 20 kPa and 30 kPa.

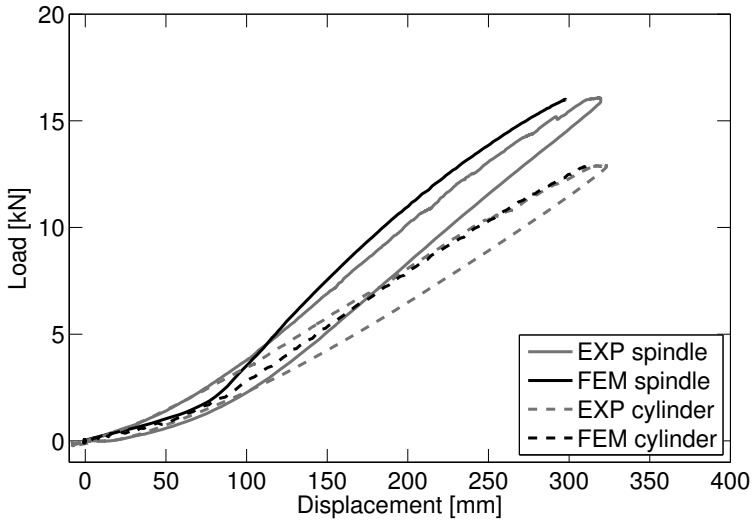

Fig. 21 Load-displacement behavior at the center of the compression member for the cylinder and the asymmetric spindle under homogeneous distributed load for 20 kPa

The load-displacement curve at midspan for a homogeneous load at 20 kPa air pressure is shown for the cylinder and the spindle in Fig. 21. The cylinder clearly shows a softer behavior. A good correlation between experimental and FEM results is found for the cylinder, too. The slope for the spindle and the

cylinder for all three load cases are given in Fig. 22 for an air pressure of 20 kPa. The spindle is in the order of 20% stiffer than the cylinder for all load cases. The results for all air pressure values are summarized in Tab. 2.

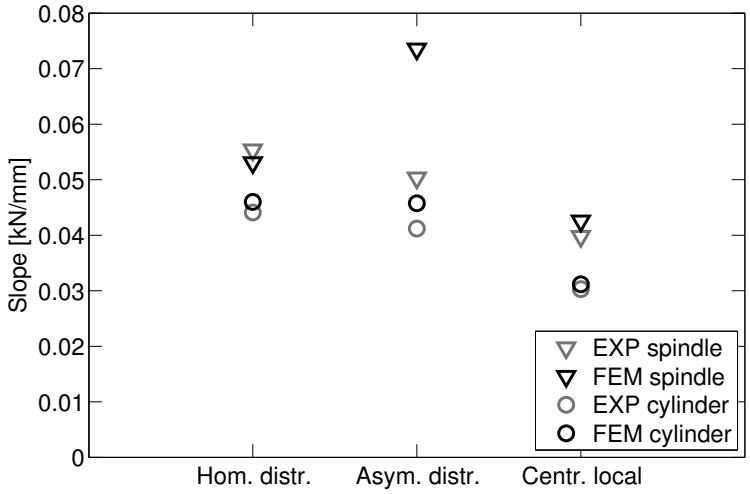

Fig. 22 Slope for the cylinder and the spindle for 20 kPa under homogeneous distributed load

		10 kPa	20 kPa	30 kPa	40 kPa
Hom. distr. load	Spindle Exp	0.043	0.055	0.077	0.092
	Spindle FEM	0.029	0.053	0.074	0.091
	Cylinder Exp	0.032	0.044	0.058	-
	Cylinder FEM	0.030	0.046	0.059	-
Sym. loc. load	Spindle Exp	0.031	0.040	0.049	0.055
	Spindle FEM	0.027	0.043	0.052	0.057
	Cylinder Exp	0.023	0.030	0.035	-
	Cylinder FEM	0.022	0.031	0.037	-
Asym. distr. load	Spindle Exp	0.038	0.050	0.061	0.072
	Spindle FEM	0.048	0.074	0.091	0.100
	Cylinder Exp	0.030	0.041	0.055	-
	Cylinder FEM	0.032	0.046	0.057	-

Table 2 Slopes of the load-displacement curves at the beam centre for all load cases and air pressure values of the cylinder and the asymmetric spindle [kN/mm].

6. Conclusions

The load bearing behavior of an asymmetric spindle shaped Tensairity girder with 8 m span was investigated. Homogeneous distributed, asymmetric distributed and central local loads were considered. The beam was tested up to an integrated homogeneous load of 18 kN and a maximal stiffness of almost 0.1 kN/mm was obtained for an air pressure of 40 kPa. The experiments show that the spindle shaped girder is stiffer for all load cases and air pressure values compared to the cylindrical girder. Good correlation was

found between experimental and FEM results obtained with a commercial software. However, the use of cables poses some challenge in the numerical modeling as the determination of the initial geometry of the cables is not trivial and the pretension of the cables has a strong influence on the deflection of the girders. The cable design demands also for several assumptions and simplifications in the presented analytical model for the homogeneous distributed load case. Nevertheless, the analytical model can well predict the stiffness of the beam as a function of the air pressure. The linear approximation of the analytical model suggests that the vertical displacement of the compression element of the Tensairity girder is basically the sum of the displacement due to the elasticity of the tension element and the displacement due to the pressure dependent constriction of the inflated hull. The stiffness of the girder can be controlled by the air pressure. Tensairity structures are adaptive structures. For local loads and asymmetric distributed loads, the horizontal force is not constant along the length of the chords and corresponding analytical models are subject of further studies. The tested girders were built for a car bridge to demonstrate the outstanding properties of Tensairity such as compact transport volume, fast set up, light weight and high load bearing capacity. The current study shows that reliable predictions of the structural behavior of Tensairity girders can be obtained with numerical and analytical methods fostering the design of civil engineering applications such as roof structures and bridges.

Acknowledgements

The authors want to thank First Entertainment for initiating the project and for the perfect opportunity to show the potential of Tensairity to a wide audience. A special thank goes to Uwe Teutsch and the team of the Bauhalle at Empa for their support during the experiments. The financial support of Festo is gratefully acknowledged.

References

[1] Topping AD. Shear deflections and buckling characteristics of inflated members. Journal of Aircraft 1963; 1(5): 289-292.

[2] Douglas WJ. Bending stiffness of an inflated cylindrical cantilever beam. AIAA Journal 1969; 7(7): 1248-1253.

[3] Comer RL, Levy S. Deflections of an inflated circular-cylindrical cantilever beam. AIAA Journal 1962; 1(7): 1652-1655.

[4] Webber JPH. Deflections of inflated cylindrical cantilever beams subjected to bending and torsion. Aeronautical Journal 1982; 86(10): 306-312.

[5] Main JA, Peterson SW, Strauss AM. Load-deflection behavior of space-based inflatable fabric beams. Journal of Aerospace Engineering 1994; 7(2): 225-238.

[6] Veldman SL, Bergsma OK, Beukers A. Bending of anisotropic inflated cylindrical beams. Thin Wall Structures 2005; 43(3): 461-475.

[7] Oden JT, Sato T. Finite strains and displacements of elastic membranes by the finite element method. International Journal of Solids and Structures 1967; 3(4): 471-488.

[8] Kyriakou SK, Schwab C, Humphrey JD. Finite element analysis of nonlinear orthotropic hyperelastic membranes. Computational Mechanics 1996; 18(4): 269-278.

[9] Wielgosz C, Thomas JC. An inflatable fabric beam finite element. Communications in Numerical Methods in Engineering 2003; 19(4): 307-312.

[10] Luchsinger RH, Pedretti A, Steingruber P, Pedretti M. The new structural concept Tensairity: Basic principles. In: A. Zingoni (Ed.), Progress in Structural Engineering, Mechanics and Computations, A.A. Balkema Publishers, London (2004).

[11] Pedretti M, Luscher R. Tensairity-Patent – Eine pneumatische Tenso-Struktur. Stahlbau 2007; 76(5): 314-319.

[12] Breuer JCM, Luchsinger RH. Inflatable kites using the concept of Tensairity. Aerospace Science and Technology 2010; in press.

[13] Plagianakos TS, Teutsch U, Crettol R, Luchsinger RH. Static response of a spindle-shaped Tensairity column to axial compression. Engineering Structures 2009; 31(8): 1822-1831.

[14] Wever TE, Plagianakos TS, Luchsinger RH, Marti P. Effect of fabric webs on the static response of spindle-shaped Tensairity columns. Journal of Structural Engineering 2010; 136(4): 410-418.

[15] Luchsinger RH, Crettol R. Experimental and numerical study of spindle shaped Tensairity girders. International Journal of Space Structures 2006; 21(3): 119-130.

[16] Luchsinger RH, Teutsch U. An analytical model for Tensairity girders. Proceedings of the 50th Anniversary Symposium of the International Association for Shell and Spatial Structures IASS 2009, Valencia, Spain.

[17] The Tensairity demonstration bridge was featured in “Die grosse Show der Naturwunder” in the German programme ARD on Sept. 27th, 2007.

[18] Luchsinger RH, Crettol R, Plagianakos TS. Temporary structures with Tensairity. Proceedings of the International Symposium IASS-SLTE 2008, 3rd Latin American Symposium on Tensile-Structures, Acapulco, Mexico.

[19] Galliot C, Luchsinger RH. A simple model describing the non-linear biaxial tensile behavior of PVC-coated polyester fabrics for use in finite element analysis. Composite Structures 2009; 90(4): 438-447.

[20] Teutsch U. Tragverhalten von Tensairity Trägern. Dissertation ETH Zürich 2009; No. 18679.

[21] Pedretti A, Steingruber P, Pedretti M, Luchsinger RH. The new structural concept Tensairity: FE-modeling and applications. In: A. Zingoni (Ed.), Progress in Structural Engineering, Mechanics and Computations, A.A. Balkema Publishers, London (2004).